Primljen / Received: 21.6.2019.
Ispravljen / Corrected: 11.4.2020.
Prihvaćen / Accepted: 30.4.2020.
Dostupno online / Available online: 10.5.2022.

Design method and engineering application of shear wall with friction energy dissipation damper

Authors:

Bin Dang, MSc. CE
Shangluo University, Shaanxi, China
College of Urban, Rural Planning and Architectural Engineering
bind@slxy.edu.cn

Assist.Prof. **Tao Li**,PhD. CE
Shangluo University, Shaanxi, China
College of Urban, Rural Planning and Architectural Engineering
Huanghuai University, Henan,China
School of Architectural Engineering
litao623114@126.com
Corresponding author

Prof. **Sheliang Wang**, PhD. CE
Xi'an University of Architecture and Technology, China
School of civil Engineering
554299675@qq.com

Assoc.Prof. **Meng Zhan**, PhD. CE
Huanghuai University, Henan,China
School of Architectural Engineering
zhanyi313@163.com

Research Paper

Bin Dang, Tao Li, Sheliang Wang, Meng Zhan

Design method and engineering application of shear wall with friction energy dissipation damper

At present, the target of seismic strengthening is to gradually work towards the objective of being able to quickly restore function, and even replace function after an earthquake. In addition, the foot of reinforced concrete shear walls is easily damaged in shear wall structures. If a damper is set in this part, it can ensure the normal stiffness and energy consumption function of the shear wall, and it can be easily and conveniently replaced after an earthquake at a low cost, which is an important measure to realize recoverable functional cities. Therefore, a new type of friction energy dissipation damper has been designed. First, the components of the damper are described, and the design process, including the base placement area, bolt hole length, and initial slip force, is theoretically analysed. Then, on the basis of a shear wall test, SAP2000 is used to analyse and verify correctness of the model. Furthermore, the dampers are placed in the corner of the shear wall for remodelling. Considering different bolt hole lengths, the hysteretic performance, bearing capacity attenuation, stiffness degradation, and energy dissipation capacity of the model are compared and analysed. The results show that the friction energy dissipation damper can improve the energy dissipation capacity and delay the stiffness degradation and bearing capacity attenuation of the structure. This study provides a theoretical basis for a more detailed engineering design and application.

Key words:

friction energy dissipation, plastic hinge, finite element analysis, bearing capacity attenuation, stiffness degradation, energy dissipation

Prethodno priopćenje

Bin Dang, Tao Li, Sheliang Wang, Meng Zhan

Metoda projektiranja i inženjerska primjena posmičnih zidova s tarnim prigušivačem seizmičke energije

U današnje je vrijeme zadatak seizmičkog pojačavanja konstrukcija postupno ostvarivanje ciljeva koji omogućuju brzo obnavljanje funkcionalnosti građevina, te čak i njihovu prenamjenu nakon potresa. Osim toga, u građevinama s posmičnim zidovima lako dolazi do oštećenja podnožja armiranobetonskih posmičnih zidova. Ako se na to mjesto postavi prigušivač, osigurava se normalna sposobnost posmičnog zida u pogledu krutosti i trošenja energije, a sam prigušivač se može jednostavno, prikladno i financijski povoljno zamijeniti nakon potresa, što je značajan faktor u razvoju gradova s obnovljivim funkcijama. U tu je svrhu projektiran novi tip prigušivača u kojem se energija troši trenjem. Na početku se opisuju komponente prigušivača te se teoretski analizira postupak projektiranja, uključujući i definiranje mjesta na koje se prigušivač postavlja, dužinu rupe vijka te početnu silu klizanja. Zatim se na temelju ispitivanja posmičnih zidova programom SAP2000 proračuna i provjerava ispravnost modela. Nakon toga se prigušivači postavljaju u kut posmičnog zida radi ponovnog modeliranja. Za razne dužine rupe vijka, u radu se uspoređuju i analiziraju histerezna učinkovitost, smanjenje nosivosti, smanjenje krutosti te učinak modela u pogledu disipacije energije. Rezultati pokazuju da se primjenom tarnog prigušivača može poboljšati trošenje energije te odgoditi smanjenje krutosti i nosivosti građevina. U radu je prikazana teoretska osnova za detaljnije inženjersko projektiranje i primjenu.

Ključne riječi:

disipacija energije trenjem, plastični zglob, analiza konačnih elemenata, smanjenje nosivosti, raspršivanje energije

1. Introduction

The goal of seismic resistance in traditional engineering structures, based on improving the seismic performance of the structure itself, is to achieve the ability to withstand earthquake disasters by developing high-performance structural materials, high-performance structural components, and high-performance structural systems [1]. Recently, due to frequent occurrence of large earthquakes worldwide, the randomness and contingency of damage intensity, it is difficult to reinforce and repair buildings after earthquakes according to the artificial assumption that "buildings can be repaired after large earthquakes", which poses a challenge to traditional seismic design. Therefore, energy dissipation and seismic reduction structures, which can be installed on some easily damaged components of the structure, have emerged. In small earthquakes, such elements can consume seismic energy, while in large earthquakes or extraordinarily large earthquakes, they will destroy themselves and consume energy to reduce excessive damage and additional deformation to the main structure [2, 3]. Currently, commonly used energy dissipation elements include metal dampers, tuned mass/liquid dampers, viscoelastic /viscous dampers, and friction dampers.

Caladod and Chen [4-6] connected the flange and web of an I-shaped steel beam with the column flange using an additional angle steel at the frame joints, to achieve the real "articulation" and dissipate energy by using the deformation of the connection angle steel. However, it was found that as the hysteretic cycle times increased, the steel plate underwent severe compressive buckling, which led to serious kneading of the hysteretic curve and weakening of the energy dissipation capacity. Guo Wei [7] started with the basic mathematical model of a tuned liquid damper (TLD). The coupling calculation of a nine-story steel structure was carried out by adding grilles in the water tank and using OpenSees and MATLAB. It was pointed out that the TLD with grilles had an adjustable and good shock absorption effect. Chen Min [8] put a viscous liquid damper onto the frame support layer of a ten-story frame-supported shear wall structure, and carried out an elastic time history analysis to ensure the safety of the shear wall structure.

Friction dampers have been studied by many experts and scholars, and have even been applied in bridges and buildings because of their strong energy consumption, unnecessary external energy support, and low maintenance cost. Therefore, these dampers are widely used in wood structures, steel structures and concrete structures. Hashemi [9, 10] carried out experiments and a numerical simulation analysis on the seismic performance of a self-resetting timber structure shear wall with a friction energy dissipation damper. Yoshiaki [11] designed three different kinds of friction connectors, placed them into the shear wall structure, carried out a simulation test of the related components, and finally established that the shear wall with friction connectors had a good energy consumption effect. Deng et al [12] introduced frictional energy dissipation dampers in the plastic hinge area of the fully prefabricated steel frame beam-column joints, and measured the energy consumption and deformation capacity of four full-scale specimens. Brian G. Morgen [13] conducted a seismic design for an unbonded post-tensioning precast concrete frame structure with a friction energy dissipation damper, and proposed the calculation principle of the initial sliding force of the friction damper and the area of the post-tensioning reinforcement on the premise of ensuring the specified design lateral stiffness and energy dissipation requirements. Liu Yunshuai [14] studied the seismic isolation performance of self-reset friction dampers. Liu Shaobo [15] developed a foam aluminium/polyurethane composite friction damper, which had the dual characteristics of a viscoelastic damper and a friction damper. Zhang Yanxia [16] proposed a kind of self-resetting and non-repairing friction energy dissipation support with prestressing steel strands and a friction damper, and carried out low-cycle reciprocating loading tests under different working conditions. Most previous literatures only studied the theory and simulation of friction energy dissipation dampers. Few studies have been done on the application of dampers to structures.

With continuous increase in population and improvement of living standard, modern architecture usually presents a three-dimensional development trend. Frame-shear walls and shear wall structures have become the mainstream of daily architecture. Many studies have shown that the foot plastic hinge part will yield when subjected to seismic load, which will lead to bar yielding and concrete destruction in this area, and to development of a high stress concentration area [17-19]. Therefore, to achieve repairable buildings, it is necessary to make the foot of the wall replaceable in a certain area. Professors Lv Xilin and Jiang Huanjun of Tongji University have made a pioneering study on this issue [20-22]. Theoretical and experimental studies on replaceable footings composed of laminated rubber pads and mild steel have been carried out. Therefore, a frictional energy dissipation damper with a convenient assembly and low cost is installed at the wall foot. This paper mainly studies its theoretical design method, deformation performance and energy dissipation capability, and presents a solid theoretical foundation for later experimental research and engineering application.

2. Composition of the friction energy dissipation damper

To realize the restorable function of a shear wall and reduce the damage accumulation in key parts, a special friction energy dissipation damper device is set up, as shown at Figure 1.

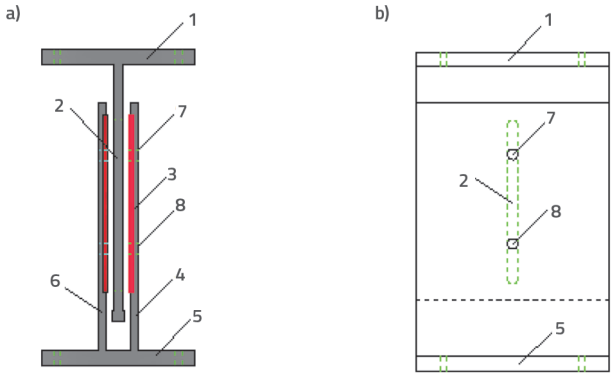

Figure 1. Design of a friction energy dissipation damper: a) Profile design; b) Elevation design

As shown in Figure 1, the frictional energy dissipation damper is mainly composed of three parts, including the inner plate 2, the frictional plate 3 and the outer plate 4(6). Both the inner and outer plates are made of high strength steel, and a brass plate is used for the friction plate. The upper end of the inner plate is fixed with the upper roof by bolts, and the lower end is free. Both sides of the middle part of the outer plates are grooved and connected with the lower floor, which is fixed with the lower components of the shear wall with bolts. The friction plate is embedded in the outer plates on both sides, and is higher than the inner surface of the outer plates. The inner plates have a long bolt hole. The outer plates and the friction plates are connected with the inner plates through two high strength bolts with anti-relaxation components. The device has the advantages of a simple structure, convenient processing, a self-resetting ability depending on the self-weight, a low cost and convenient replacement. The device is suitable for the energy dissipation and vibration reduction of structures.

3. Design theory of the friction energy dissipation damper at wall foot

3.1. Determination of resettlement area size

Under strong earthquakes, the wall foot is the most severely damaged area and, according to the flat section assumption and the deformation coordination principle, the plastic deformation is the largest at the wall foot, which is the so-called plastic hinge region [23, 24]. In other words, the region length is an important index of the ductility and energy dissipation capacity of reinforced concrete (RC) shear walls. Therefore, the size of the replaced area is initially determined to be no less than that of the plastic hinge area.

Domestic and international scholars, including Park [25], Paulay [26], Bohl [27] and Qian Jia-ru [23], have studied the calculation model and influencing factors of the plastic hinge length with reinforced concrete shear walls since the 1950s. However, due to a large number of factors affecting its length, the focus of the researchers' attention has been different. No unified conclusion has been drawn so far, although a large number of experimental studies, theoretical analyses and numerical simulations have been carried out on the plastic hinge length of shear wall structures. Table 1 shows the results of research on the length of plastic hinges as conducted by some experts and scholars at home and abroad.

Table 1. Formulas for calculating the equivalent plastic hinge length of an RC shear wall

Literature	Computational model
[24]	$l_p = (2{,}5 \approx 3{,}0) \cdot b_c$
[25]	$l_p = 0{,}5 \cdot h_w$
[26]	$l_p = 0{,}2 \cdot h_w + 0{,}44 \cdot H_w$
[27]	$l_p = (0.2 \cdot h_w + 0.05 \cdot z) \cdot (1 - 1.5 \frac{P}{f_c' b_c h_w})$ $l_{pz} = 0.48 h_w \lambda^{0.35} (1 - \mu_N)(1 - 14.87 \rho_v)$
[28]	$l_p (H_w - \frac{1}{2} l_p) = l_{pz} (\frac{1}{2} H_w - \frac{1}{3} l_{pz})$
[29]	$l_p = (0{,}33\ m - 0{,}03) \cdot H_w$
[30]	$l_p = 0.43 \cdot h_{w0} + 0.077 \cdot \frac{H_w}{h_{w0}}$

Remarks: f'_c, l_{pz}, λ, m', μ_N, ρ_v and h_{w0} denote the compressive strength of concrete cylinders, the plastic hinge length, the shear span ratio, the bending shear ratio, the axial compression ratio, the stirrup ratio and the effective section height of an RC shear wall, respectively, while the remaining parameters given in the table are shown in Figure 2.a.

References [21, 23] suggest that the relatively simple and practical calculation method in reference [26] is adopted in this paper. The calculated length of the plastic hinge is as follows:

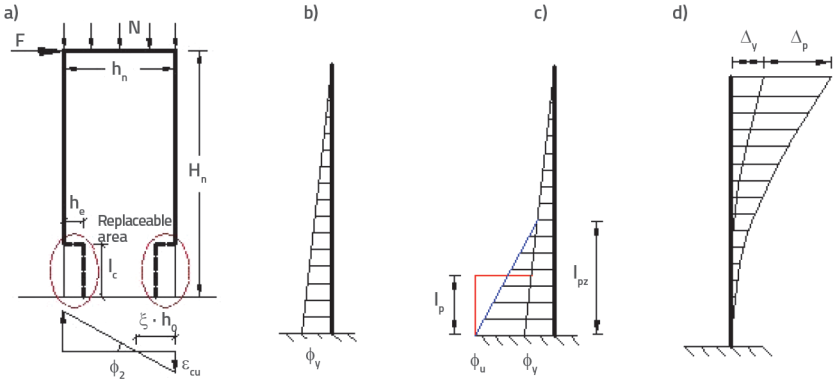

Figure 2. Force deformation diagram of a cantilever shear wall: a) Force diagram; b) Yield curvature; c) Limit curvature; d) Deformation diagram

$$l_c = \gamma_1 l_p = \gamma_1(0{,}2\cdot h_w + 0{,}044\cdot H_w) \quad (1)$$

As demonstrated in Figure 2, the concentrated plastic hinge model of the bottom section with bending failure is used for calculation. $\varepsilon_{c,max}$, ϕ_u and ξ denote the ultimate compressive bending of concrete at the edge of the compression zone, the maximum section curvature, and the relative pressure zone height, respectively. Assuming that the shear wall is at the limit state, the section curvature in the lower equivalent plastic hinge area l_p is the same [25], that is to say $\phi_p = \phi_u - \phi_y$, where $-\phi_y$ represents the yield curvature of the bottom section.

For an un-opened shear wall, it can be simplified to the calculation of the cantilevered member. Based on mechanics and the above assumptions, the ultimate displacement angle is:

$$\theta_u = \frac{1}{3}\phi_y H_w + (\phi_u - \phi_y) l_p \quad (2)$$

Normally $(1/3)(\phi_y H_w) - \phi_y l_p < \phi_u l_p$ [21]. Therefore, when the bottom section of the RC shear wall reaches the ultimate curvature, the ultimate compressive strain of concrete is:

$$\varepsilon_{c,\max} = \phi_u \cdot \xi h_0 \approx \frac{\theta_u \xi h_0}{l_p} \quad (3)$$

Assuming that replaceable components are needed in the area where the concrete strain is exceeded, the replaceable area width can be obtained:

$$h_c = \gamma_2 h_p = \gamma_2\left(1 - \frac{\varepsilon_x}{\varepsilon_{cu}}\right)\xi h_0 = \gamma_2\left(1 - \frac{\varepsilon_x l_p}{\theta_u \xi h_0}\right)\xi h_0 \quad (4)$$

In the above formulas γ_1 and γ_2 are the comprehensive influence coefficients, which take into account the initial defects of the concrete members, the accidental eccentricity, the installation error, and other factors. This value can be selected according to the importance of the structure or component.

3.2. Determination of displacement ductility ratio

It can be obtained from Figure. 2.d that the cross-sectional displacement ductility ratio and the curvature ductility ratio are defined respectively, as shown in Eq. (5):

$$\mu_\Delta = \frac{\Delta_u}{\Delta_y} = \frac{\Delta_y + \Delta_p}{\Delta_y} \quad (5)$$

$$\mu_\phi = \frac{\phi_u}{\phi_y} \quad (6)$$

where Δ_y, Δ_u and Δ_p are the yielding displacement, the ultimate displacement, and the plastic displacement at the ultimate state of the RC shear wall, respectively.

When the bottom of the shear wall has just yielded, the curvature of the section can be considered to vary linearly along the height of the shear wall. The relationship between the top displacement of the cantilever shear wall and the curvature is as follows:

$$\Delta = \iint \phi(x)dxdy = \iint \frac{x}{H}\phi_y dxdy \quad (7)$$

Assume that when the limit state is reached, the centre point of the equivalent plastic hinge area is the plastic rotation centre, and the plastic displacement can be obtained as:

$$\Delta_p = \phi_p(H_w - 0.5l_p) = (\phi_u - \phi_y)l_p(H_w - 0.5l_p) \quad (8)$$

The method in mechanics is available:

$$\Delta_y = \frac{1}{3}F_y H_w^3 = \frac{1}{3}\phi_y H_w^2 \quad (9)$$

Therefore,

$$\mu_\Delta = \frac{\Delta_u}{\Delta_y} = \frac{\Delta_y + \Delta_p}{\Delta_y} = 1 + \frac{(\phi_u - \phi_y)l_p(H_w - 0.5l_p)}{\frac{1}{3}\phi_y H_w^2} = 1 + 3(u_\phi - 1)\frac{l_p}{H_w}\left(1 - 0.5\frac{l_p}{H_w}\right) \quad (10)$$

Theoretically, equation (7) can be integrated to obtain the bottom section curvature and vertex displacement of the shear wall, but the theoretical calculation results are usually not consistent with the experimental measurements [31]. Based on the conclusions of Priestley [32], Professor Qian Jiaru [23] and Professor Liang Xingwen [23], the yield curvature and ultimate curvature can be obtained from:

$$\begin{cases} \phi_y = 3\cdot\dfrac{f_y}{E_s \cdot h_w} \\ \phi_u = \dfrac{\varepsilon_{c,\max}}{\xi \cdot h_{w0}} = \dfrac{\varepsilon_{cu}}{\dfrac{N + \rho_w b_w h_{w0} f_{yv}}{\alpha_1 f_c b_w \beta + 2\rho_w b_w f_{yv}}} \end{cases} \quad (11)$$

where ε_{cu} is the ultimate compressive bending of concrete and, as stipulated in reference [33], is: $\varepsilon_{cu} = 0{,}0033 - (f_{cu,k} - 50)\cdot 10^{-5}$. The displacement ductility ratio can be obtained by substituting the calculation result of Formula (11) into Formulas (6) and (10).

3.3 Determination of bolt hole length

The displacement ductility ratio reflects the ratio of displacement to the yield displacement when the top structure is destroyed. At the same time, the relationship between the displacement of the wall top and the lifting distance of the wall foot can also be used in calculations [34], that is,

$$\mu_{SF} = \frac{\Delta_y + \Delta_s}{\Delta_y} \le \mu_\Delta \quad (12)$$

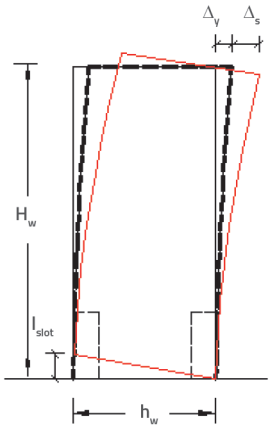

Figure 3. Relationship between top displacement and foot lifting distance

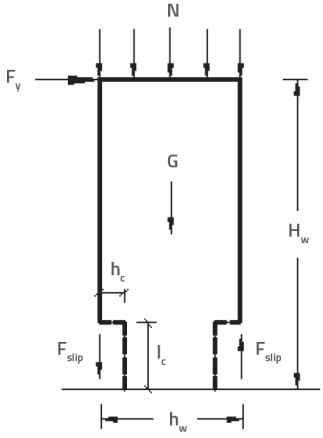

Figure 4. Force diagram of the shear wall structure during initial slip

From Figure 3, it is assumed that the angle at which the wall foot rises is the same as that around the bottom, after the top yields. Therefore,

$$\Delta_s = I_{slot} \cdot \frac{H_w}{h_w} \tag{13}$$

By substituting Formula (13) into Formula (12), it can be concluded that:

$$I_{slot} = (\mu_\Delta - 1) \cdot \Delta_y \cdot \frac{h_w}{H_w} \tag{14}$$

3.4. Determination of initial slip force

When the outermost steel bar at the wall foot initially yields, the wall friction energy damper starts to slip. The horizontal force applied on the wall top is *Fy*, which is also defined as the yield load of the shear wall, as shown in Figure 4. F_{slip} is the vertical force value when the damper starts to slip. The equilibrium equation for the force of Figure 4 is available:

$$F_{slip} = \frac{F_y H_w}{h_w} - \frac{N+G}{2} \tag{15}$$

where N is the axial force applied to the shear wall by the superstructure, which can be determined by the axial compression ratio, and G is the self-weight of the shear wall itself.

Scholars usually study yield loads with great discreteness. Therefore, they usually research the ultimate loads first, and then transform them into yield loads by fitting the relationship between tests. In this paper, the experimental fitting results of the variable-parameter shear wall members are given by Professor Lv Xilin [29], as shown in Formula (16).

$$\frac{F_u}{F_y} = 2.05 - 0.31n + 0.40\lambda_v - 0.34\lambda \tag{16}$$

where n, λ_v and λ are the axial compression ratio, the bracing characteristic value of the edge member, and the shear span ratio of the shear wall, respectively.

For large eccentric compression shear walls, when the concrete compression edge fibre reaches the limit state, the reinforced concrete shear wall structure is assumed to reach the limit state, and the concrete strain pattern is equivalent to the triangle [35], as shown in Figure 5.

Figure 5.b is artificially divided into three parts, namely, two congruent triangular parts (a) and (b), and a trapezoidal part (c). In the first two, the tension is equal to the horizontally distributed steel bar of the shear wall under pressure, and its stress bending approximation is equal. In other words, when considering the force balance in horizontal direction, the stresses of the horizontally distributed steel bars in the two triangular areas cancel each other, and are not calculated. In the remaining part (c), the strain of the horizontally distributed reinforcement is close to the rectangular distribution, within which all the reinforcements yield, Eq. (17):

$$\begin{cases} M = F_u H_w \\ M + \rho_w b_w h_{w0}(1-2\xi_u) f_{yv} \cdot \frac{1}{2} h_{w0}(1-2\xi_u) - f_y' A_s'(h_{w0} - a_s') - \\ -N \cdot (\frac{h_w}{2} - a_s) - \alpha_1 f_c b_w \beta \xi_u h_{w0}(h_{w0} - \frac{1}{2}\xi_u h_{w0}) = 0 \end{cases} \tag{17}$$

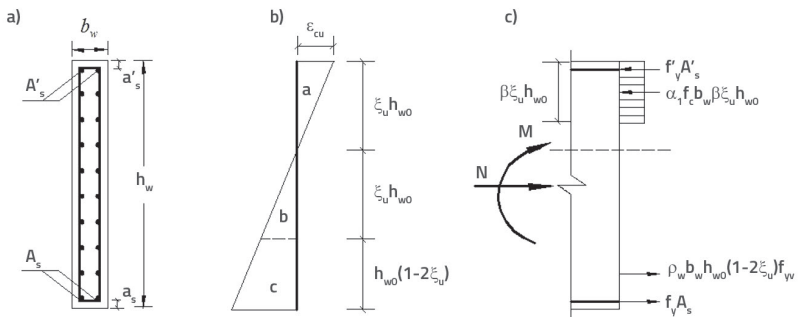

Figure 5. Force analysis diagram of a shear wall: a) cross section; b) strain distribution; c) force balance

The value of F_y can be obtained from the Eq. (17), and this value can then be substituted into equation (15) to obtain F_{slip}.

3.5. Determination of bolt preload

The initial slip force F_{slip} of the bolt is the maximum static friction between the steel plate and the friction plate, therefore,

$$F_{slip} = \mu \cdot n_s \cdot n_b \cdot T_b \quad (18)$$

gdje je μ koeficijent trenja između tarne ploče i unutarnje ploče, Where μ is the friction factor between the friction plate and the inner plate, which can be based on experience or test values; n_s and n_b are the slip surfaces number and bolt number, respectively, and T_b is the pulling force applied by only one bolt.

3.6. Determination of the number of shear bolts

The formula for calculating the number of bolts is as follows:

$$n = \frac{F_{slip}}{\min(N_v^b, N_c^b)} \quad (19)$$

where N_v^b and N_c^b are the shear and bearing capacity of the bolts, respectively, which are designed in accordance with the Chinese code "Standard for design of steel structures (GB 50017-2017)".

The above equations can be used as a guideline for designing the replaceable shear wall member as a more accurate calculation modelling can thus be achieved. Numerical simulation models based on these formulas are presented in the following section.

4. Model validation

The general contrast wall (SW-0) presented in reference [20] is used as an example, and its dimensional characteristics are shown in Table 2. Among them, the longitudinal reinforcement of concealed columns is grade II, and the horizontal reinforcement, vertical reinforcement, and stirrups of the concealed columns are grade I.

The non-linear layered shell element [36] is adopted. This element divides the steel bar and concrete structure into many layers by the finite element software SAP2000, one of the many available simulation programs. This software can take into account the coupling between in-plane bending, in-plane shear and out-of-plane bending, and it can fully reflect spatial mechanical properties of shell structures. The stress-strain constitutive curve of concrete adopts the "Mander model", which can consider the influence of stirrups. Another important material, the steel bar, adopts the double-folded line model and "kinematic" hysteretic model.

When the lateral displacement of a shear wall is small, the shear value borne by the damper at the foot of the wall is less than F_{slip}, that is, the damper has not yet slipped, and an elastic-plastic deformation occurs between the internal friction plate and the external friction plate. When the shear force of the damper reaches F_{slip}, the damper begins to slide. At this time, the shear force of the damper remains constant. When sliding to the upper (lower) end of the long bolt hole, the shear force will increase linearly, because the hole wall is blocked. The reverse

Table 2. Size and reinforcement characteristic values of reinforced concrete shear wall

Type	Characteristic value
Wall section size (height × length × width)	3200 mm × 1600 mm × 200 mm
Loading steel plate size	500 mm × 450 mm × 20 mm
Loading steel plate setting method	Embedment
Distribution bar and stress bar of shear wall	Φ8/120
Shear wall tension reinforcement	Φ6/240
Strength grade of concrete	C25
Compressive strength of concrete cube	28.5 MPa

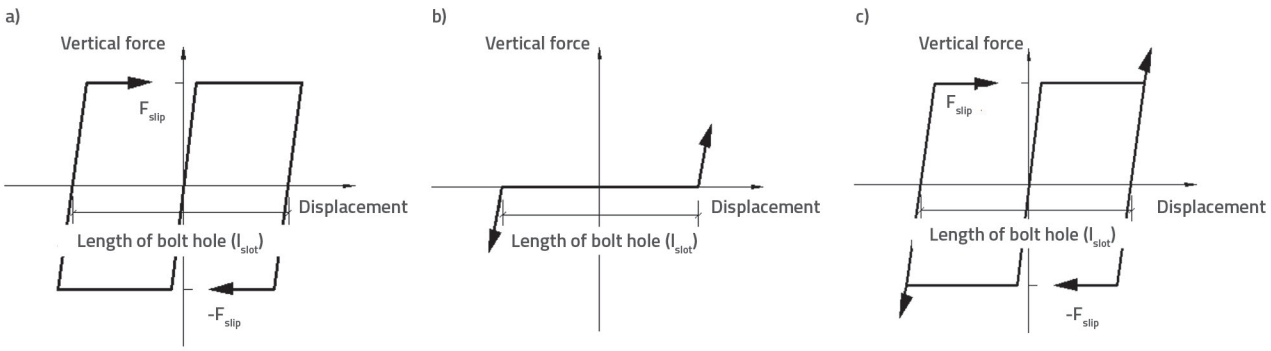

Figure 6. Force analysis diagram of a shear wall: a) Constitutive relationship of the friction-slip damper; b) Hook model; c) Coupled model

loading is similar to the case of forward loading, assuming that both unloading and reloading are performed in a linear manner (the stiffness value remains the same), and the effect of the loading history is ignored [34, 37].

Based on the above analysis, a multilinear plastic model (kinematical model) without stiffness attenuation is used to simulate the elastic-plastic characteristics of the friction sliding energy dissipation damper, as shown in Figure 6.a. In addition, the hook element is used to simulate force characteristics of the maximum lifting distance of the friction slip damper after being restricted by the long bolt hole, as shown in Figure 6.b. To sum up, the force displacement coupling characteristic model of the friction energy dissipation damper is shown in Figure 6.c. In the simulation, the start and the end of sliding are considered by defining different stiffness and displacement values. Due to the shear elastoplastic deformation, the shear stiffness of the materials is used as the basic stiffness value for simulation. With reference to the relevant literature [38, 39], the calculation formula is as follows:

$$G=\frac{E}{2(1+\nu)} \tag{20}$$

where E and ν are the elastic modulus and Poisson's ratio of the material, respectively, and both of them are valued according to the literature [39, 40]. After calculation, the shear stiffness of brass (34.62 GPa) is used as the approximate stiffness of elastic-plastic deformation before sliding because of its lower shear modulus value compared to steel. When the sliding starts, the shear stiffness value is taken as 0. When the upward (downward) sliding reaches the 0.5 slot, the hook element starts to play a role due to blockage of the bolt hole, assuming that the shear stiffness value still increases linearly to 34.62 GPa.

In the simulation process, the length of the long bolt hole was set through the "open" property in the nonlinear analysis condition of the hook element. At the same time, a loading steel beam is set on top of the shear wall to facilitate application of vertical load. The displacement loading method given in reference [20] is adopted to simplify the analysis and comparison with test results. The loading schematic diagram for simulation is shown in Figure 7.

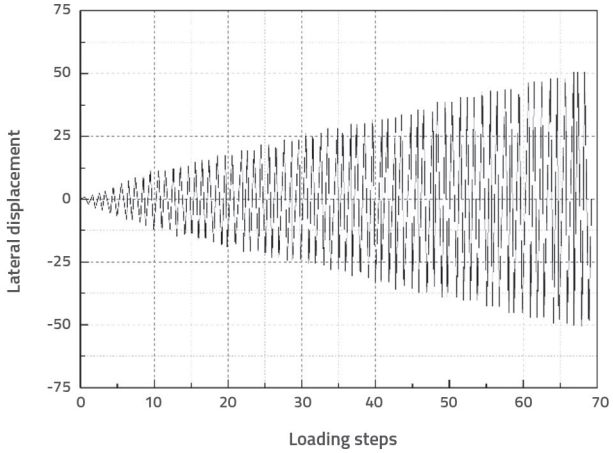

Figure 7. Schematic diagram of loading for a common shear wall

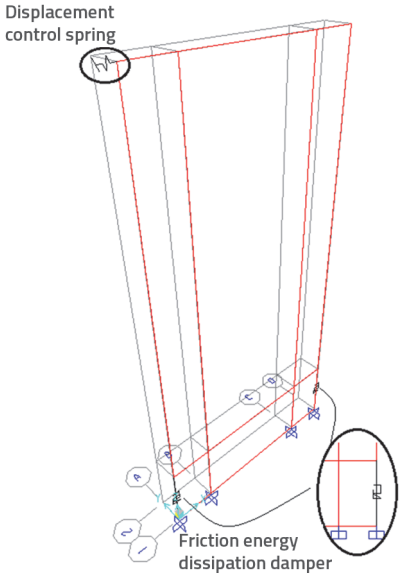

Figure 8. Schematic diagram of a shear wall structure under load

In the simulation, the "function" command is used to import the time history loading curve. Then the displacement time

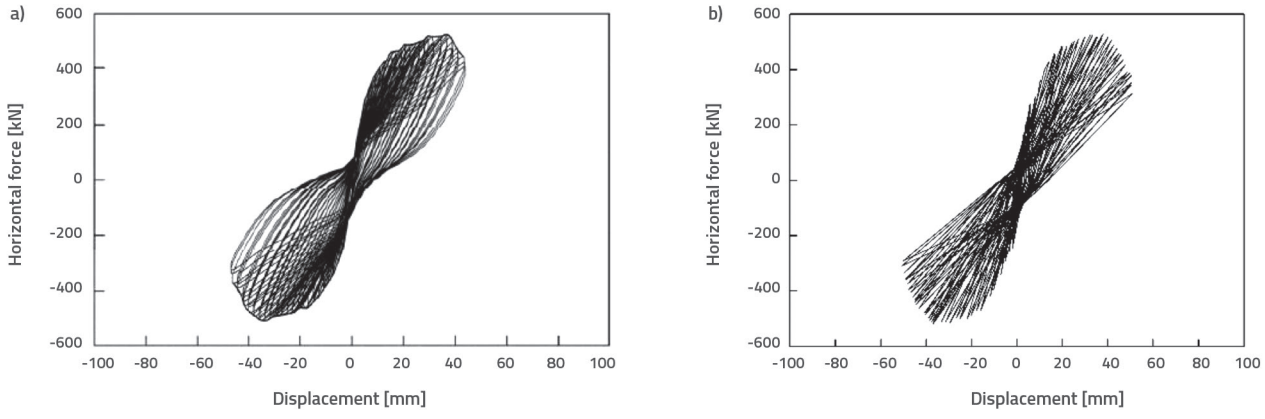

Figure 9. Contrast diagram of the hysteresis curve between the experiment and simulation: a) experimental hysteretic curve [20]; b) simulated hysteretic curve

history is applied to the shear wall by the displacement control spring with a relatively larger spring coefficient, which can also eliminate the numerical convergence problem after the shear wall ultimate load [34, 41]. The embedded columns of the shear wall and the middle part are defined as sections according to the different reinforcement methods and reinforcement ratio given in Table 2. Finally, edge restraints are generated along the object edges to establish the total finite element model. Figure 8 is a schematic diagram of the shear wall with the damper added at the bottom of the wall. After calculation and analysis, the comparison analysis diagram of the hysteretic curve, the skeleton curve and the hysteretic loops at the main characteristic values of the experiment and simulation are shown in Figure 9 and Figure 10.

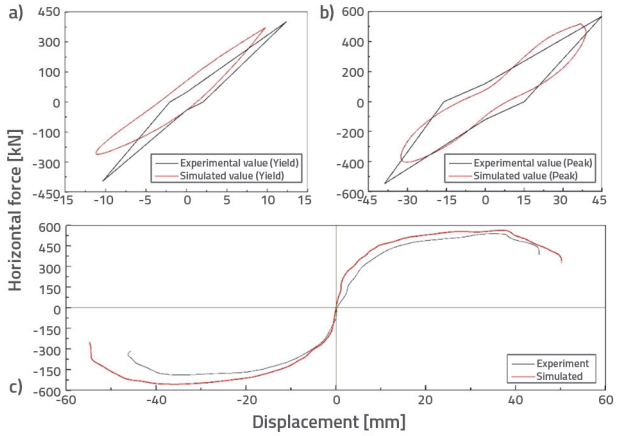

Figure 10. Comparison and verification of the hysteresis loop and skeleton curve: a) hysteresis loop at yield; b) hysteresis loop at peak point; c) skeleton curve

Because the ideal concrete elastic-plastic model is used in the simulation process, the descending section of the simulated hysteretic curve is longer than that of the actual experiment and the peak force value is also relatively larger. Due to the bar double-folded line, the kneading effect caused by the yield is not obvious. Because the ideal materials used in the simulation do not have initial defects and artificial loading errors, it can be seen from the skeleton curve that the simulated force is larger under the same level of displacement load, which intuitively shows that the contour line of the skeleton curve is higher than that of the experimental value (Figure 10.c). Accordingly, it can be seen from Figure 10.a and 10.b that the hysteresis loops of the two are similar at the main characteristic values, that is, the energy dissipation capacity at the same time is similar. In general, the model can meet the actual project needs within a certain error range and can be used to analyse an actual project.

5. Numerical analysis under different conditions

To verify the seismic performance of an RC shear wall caused by large eccentric bending, the engineering example in the above section is taken as the research object, and the frictional energy dissipation damper is manufactured using the above design theory. Preliminary parameters selected are shown in Table 3. As indicated in reference [42], each loading cycle is three times after yielding. Meanwhile, the displacement loading is simplified to facilitate observation, as shown in Figure 11.

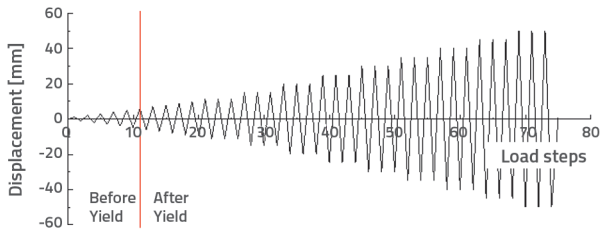

Figure 11. Displacement loading curve for simulation

Through calculation of Formulas (15) - (17) it can be determined that Fslip is equal to 118.8 kN. Combined Formulas (9) and (11) show that the yield displacement of the ordinary concrete shear wall is 11.52 mm (Δy=11.52 mm). In view of the many factors affecting ductility, four ductility coefficients (2, 3, 4, 5), commonly used in shear wall structures, are selected in this paper to enhance the applicability of different types of shear walls. Shear walls with different ductility coefficients are studied in this paper. The setting conditions are shown in Table 4.

Table 3. Basic physical parameters of the design

Type	Characteristic value
Design axial compression ratio, μ_N	0.3
Vertical pressure, N	1069 kN
Replaceable area (height × width × thickness)	500 mm × 320 mm × 200 mm
Friction plate material	brass
Friction factor between brass and steel plate, μ	0.3
Thickness of inner plate	40 mm
Thickness of outer plate	24 mm
Bolt type	M22

Table 4. Simulation condition of shear walls

NO.	Ductility coefficient	Length of long bolt hole [mm]	Corresponding lateral displacement of shear wall [mm]
1	-	-	-
2	2	5.76	23.04
3	3	11.52	34.56
4	4	17.28	46.08
5	5	23.04	57.60
Remarks: The length of the long bolt hole and the corresponding wall top lateral displacement are given in Eq. (14).			

Remarks: The length of the long bolt hole and the corresponding wall top lateral displacement are given in Formula (14).

According to the fourth section, the simulation calculations are carried out for 5 working conditions. To observe the stress changes of concrete under different working conditions, the stress nephograms (S11) of the layered shell element corresponding to the concrete cover are obtained under the same displacement (Δ = 40.56 mm), as shown in Figure 12. When the lateral displacement reaches 40.56 mm, the displacement value of the wall top is greater than that of the friction damper sliding to the top (bottom) of the long bolt hole, that is, the Hook model has played its role earlier. However, under the action of this displacement, the latter two working conditions are still in the slip stage, and have not reached the top (bottom) of the bolt hole. Figure 12 clearly shows the influence of the bolt hole length of the friction damper on the overall stress of the shear wall. For the ordinary concrete shear wall, the maximum positive and negative stresses (39.0, -45.5) appear at the foot of the wall and are also the maximum stress corresponding to the test phenomenon [17-20]. Due to the coupling of the axial force and the lateral displacement on top of the shear wall, the stress concentration phenomenon appears on the outermost side of the wall. Comparing conditions (2) and (3), the tension and compression zones of the two are basically the same, and the maximum stress of concrete occurs at the joint of the wall and the friction damper after slip. However, in the former condition, the bolt bar of the friction damper is stressed earlier, which has a greater influence on the concrete stress. For example, the maximum compressive stresses of the two are -35.0 and -32.0, which are by 23.08 % and 29.7 % lower than that of the ordinary concrete shear wall with a considerable reduction, respectively. In other words, as the friction consumes the input energy, the larger the friction distance, the more energy is consumed, and the lower is the stress value of the concrete connected with the connector. At that moment, the damper is still sliding for conditions (4) and (5). However, due to large sliding length, lateral displacement is also large, which makes the main tension and compression area of the concrete transition from the joint to the corner of the wall. At this time, the maximum stress of concrete wall appears in the corner of the wall, and the maximum compressive stress of both is 30.0, which is lower than the above three conditions. Because of the same input and consumed energy, the range of the tension and compression zones of the concrete and the magnitude of the stress are similar.

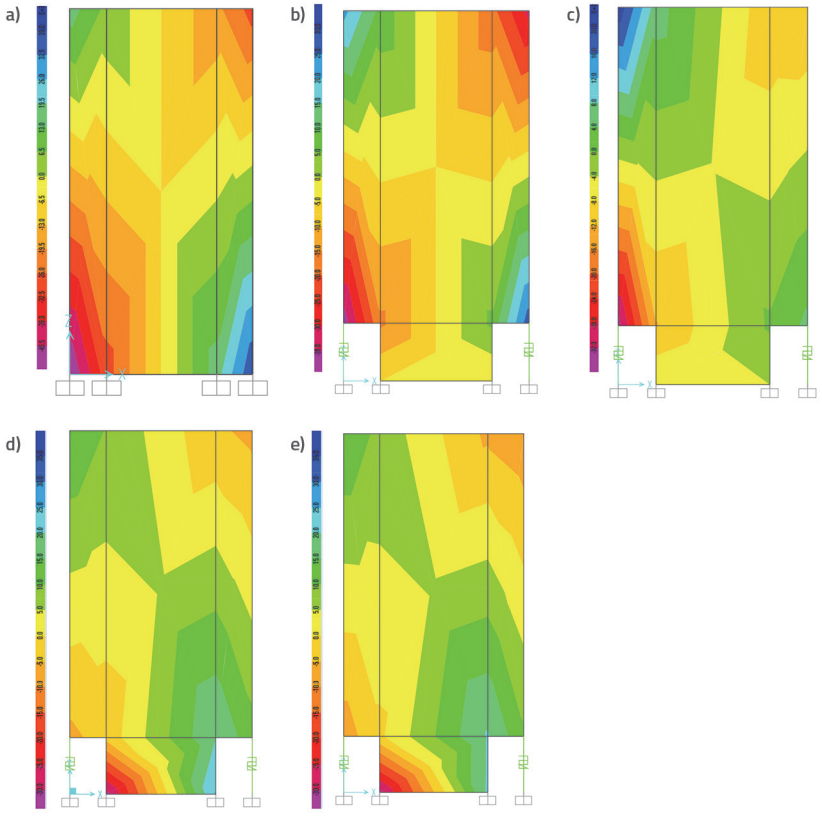

Figure 12. Stress nephogram of the shear wall corresponding to different bolt hole lengths at any time under the five conditions (Δ = 40.56 mm, S11)

At the same time, the hysteretic curves under various working conditions are also obtained, as shown in Figure 13.

As the figure above shows, the friction damper changes the shape of the hysteretic loops and makes the hysteresis curve present a "bow", but it still presents a "shuttle" before the model yielded. After that, the area of the hysteresis loop

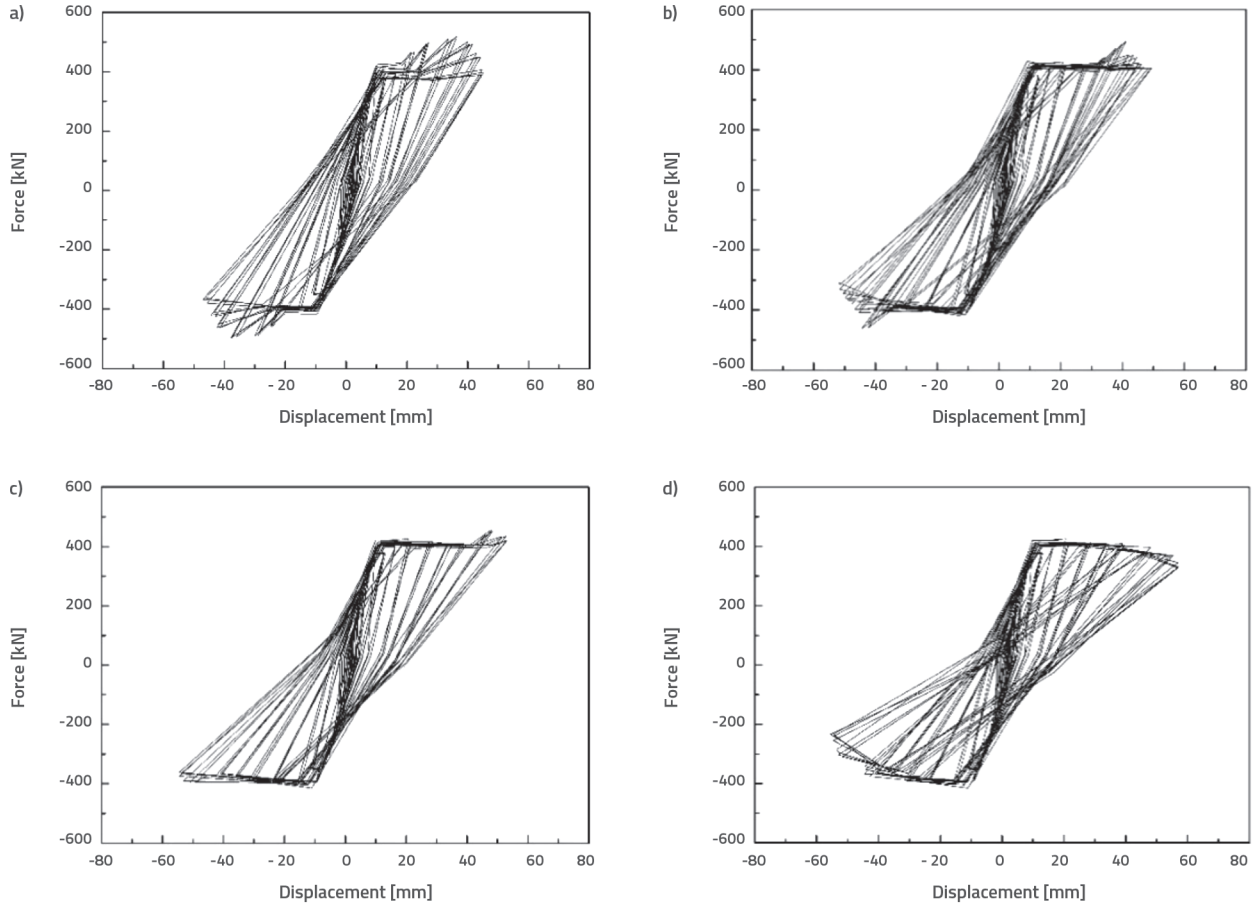

Figure 13. Hysteretic curve corresponding to different bolt hole lengths: a) Bolt hole length equal to 5.76 mm ($\mu_\Delta = 2$); b) Bolt hole length equal to 11.52 mm ($\mu_\Delta = 3$); c) Bolt hole length equal to 17.28 mm ($\mu_\Delta = 4$); d) Bolt hole length equal to 23.04 mm ($\mu_\Delta = 5$)

increases gradually, which indicates that the energy dissipation capacity of the model becomes stronger. At the same time, due to the accumulation of residual damage and deformation, the hysteresis loop inclines to some extent, and the degradation rate of strength and stiffness accelerates gradually. To clearly analyse the effect of friction dampers on concrete structures, a more detailed study of the hysteresis curve will be conducted.

6. Analysis of simulation results

6.1. Attenuation of bearing capacity

Under a given displacement amplitude, the bearing capacity of members decreases as the number of cycles increases. This kind of attenuation has a great influence on the bearing capacity of components. The faster the attenuation, the greater deterioration of seismic performance. The attenuation coefficient of the bearing capacity λ_i is generally expressed by the following formula.

$$\lambda_i = \frac{p_j^i}{p_j^{i-1}} \tag{21}$$

Where p_j^i and $p^{i-1}{}_j$ are the corresponding loads of the i and i-1 cycles under the j displacement amplitude, respectively. Using the data of the hysteretic curves, the second cycle of each stage is selected as the research object, and the influence of different bolt hole lengths on the bearing capacity attenuation is obtained, as shown in Figure 14.

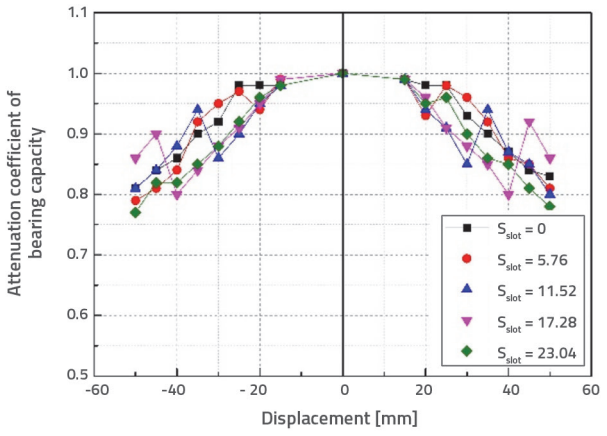

Figure 14. Influence of bolt hole length on attenuation of bearing capacity

It can be seen from the graph that the bearing capacity at different displacement points decreases as the loading cycles increase. The main reason is that the damage accumulates and the bearing capacity decreases due to the superposition of plastic deformation under loading. However, different energy dissipation also forms because of fluctuations in the attenuation of the bearing capacity and different attenuation rates. For example, when the lateral displacement is from 40 mm to 45 mm, for *Sslot*= 17.28 mm, the pure friction energy dissipation is transformed into the damper extrusion energy dissipation, and the forward bearing capacity attenuation coefficient of the model is increased from 0.8 to 0.92. Compared with a constant decrease of *Sslot*=23.04mm, the attenuation rate slows down to some extent, which guarantees the normal bearing capacity of the structure.

6.2. Stiffness degradation

The secant stiffness is used to study the stiffness attenuation laws during the repeated loading process, and the expression of the top lateral stiffness in the positive and negative loading periods is defined as in [43],

$$K = \frac{\left|P_i^+\right| + \left|P_i^-\right|}{\left|\Delta_i^+\right| + \left|\Delta_i^-\right|} \tag{22}$$

where P^+_i and P^-_i are the maximum and minimum values of the horizontal load under the i cycle, Δ^+_i and Δ^-_i are horizontal displacements corresponding to peak loads, as shown in Figure 15.

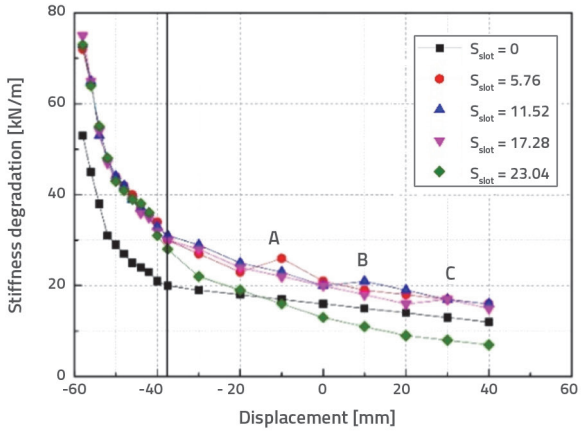

Figure 15. Influence of bolt hole length on stiffness degradation

As shown in the figure, the initial stiffness of the shear wall increases by approximately 37.8 % with the addition of the friction energy dissipation damper. Before yielding, the stiffness degradation slightly changes a litter with the bolt hole length, and the stiffness values are greater than those of ordinary concrete shear walls. After yielding, the friction energy dissipation damper begins to slip and dissipate energy. When sliding to the top, the stiffness will increase to varying degrees (points A, B and C in the figure). In other words, the existence of friction energy dissipation dampers delays the stiffness degradation of the model structure, and the stiffness values are greater than those of ordinary concrete under the same displacement. However, for *Sslot*= 23.04 mm, when sliding to the top, the theoretical lateral displacement of the shear wall should be 57.6 mm, which is greater than the maximum lateral displacement of 50 mm. It can be seen from the figure that the stiffness of the shear wall decreases rapidly. Therefore, it is necessary to avoid the occurrence of this situation in the future, to prevent the unsatisfactory application, due to excessive attenuation of stiffness.

6.3. Energy consumption capacity

The Equivalent viscous damping coefficient was proposed by Clough and Penzien [44]. It is used to quantitatively describe the comprehensive energy dissipation capacity in the process of earthquake resistance. The expression is as follows:

$$h_e = \frac{1}{2\pi} \cdot \frac{S_{ABC} + S_{ADC}}{S_{\Delta BOG} + S_{\Delta DOF}} \tag{23}$$

Where S_{ABC} + S_{ADC} is the energy dissipated by the specimen in a complete loading-unloading cycle, which can be calculated by the strip method. $S_{\Delta BOG}$ and $S_{\Delta DOF}$ are the area (i.e. the energy absorbed) that is surrounded by a hypothetical elastic structure when it reaches the same displacement. It can be obtained from experimental eigenvalues, as shown in Figure 16.

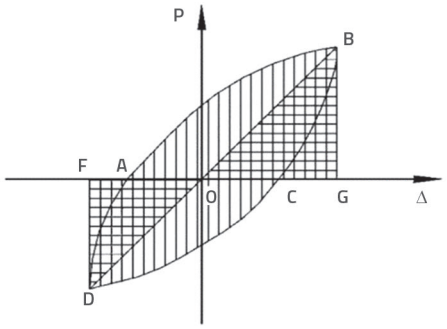

Figure16. Illustration of the equivalent hysteresis-damping-ratio

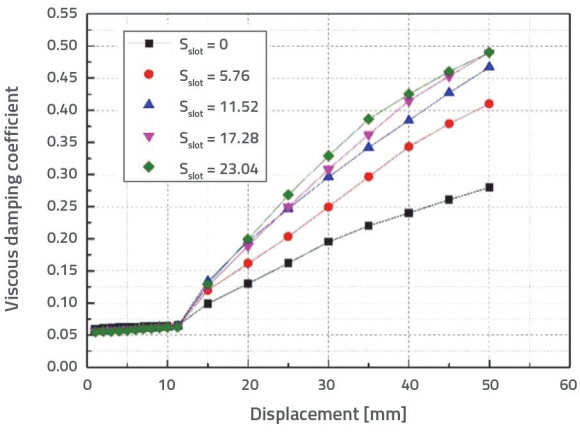

Figure 17. Effect of bolt hole length on equivalent viscous damping coefficient

Figure 17 shows the magnitude of the equivalent viscous damping coefficient calculated under different working conditions. It can be seen from the figure that, before yielding, the model plastic deformation is relatively small due to its larger stiffness, and the energy dissipation capacity increases slightly, but the change is not obvious. After yielding, the plastic deformation becomes larger, and the friction energy dissipation capacity increases gradually. However, as the number of reciprocating friction cycles increases, the local plastic materials flow between the brass plate and the steel plate. This is due to the continuous increase of the plastic deformation, which makes the friction effect worse and leads to a decrease in the slope of the trend line in the drawing. However, the energy dissipation effect increases obviously with the addition of friction dampers. For example, when the lateral displacement is 50mm, the viscous damping coefficient of an ordinary concrete shear wall is only 0.28. With the increase of the length of the long bolt holes, the viscous damping coefficient increases by 46.4 %, 66.8 %, 75 % and 75 %. The energy dissipation effect has increased remarkably.

To summarize, a reasonable design of friction dampers can make the model obtain a greater stiffness and energy dissipation capacity under the premise of ensuring a certain bearing capacity, in other words, a better seismic capacity can be obtained. At the same time, it can ensure that the model is convenient, quick and replaceable under the premise of having a little self-reset. However, further study is needed with regard to the optimisation of the length of the bolt holes on the basis of engineering practice.

7. Conclusions

A new type of RC shear wall with a friction energy dissipation damper is proposed. The shear wall has a certain self-resetting ability depending on its self-weight, and has the advantages of strong energy dissipation and easy replacement. The following conclusions can be drawn based on the analysis presented in the paper:

- Based on the theoretical analysis, the key design points such as the placement area, the initial slip force, and the long bolt hole length of this replaceable friction energy dissipation damper, are analysed and designed. The research shows that this design method has a certain reliability and can be applied in engineering practice.
- Based on the above design theory, the reinforced concrete wall is simulated by layered shell elements, and the friction sliding damper is simulated by a multi-linear plastic model and a hook model. Then, a finite element simulation analysis of a shear wall is carried out. The hysteretic curve, skeleton curve and energy dissipation capacity of the simulated and experimental values are compared and analysed, and the results show that there is no significant difference between them, that is, that the abovementioned modelling method is suitable.
- Using SAP2000 and the validated model, the energy dissipation shear walls with bolt holes with lengths of 5.76 mm, 11.52 mm, 17.28 mm and 23.04 mm are simulated and analysed, and their hysteretic capacity, bearing capacity attenuation, stiffness degradation and energy dissipation capacity are compared and analysed. The results show that the friction energy dissipation damper can improve the energy dissipation capacity of the shear wall structure, delay the stiffness degradation and bearing capacity attenuation, and be easily replaced after an earthquake.

Acknowledgements

The work presented in this paper was partially supported by Scientific Research Projects of Shaanxi Education Department (16JK1244), , Shaanxi Natural Science Foundation Project (2021JQ-844), Henan province key projects of science and technology (222102320311, 222102320199). In addition, we also want to express our gratitude to Professor Lv Xilin for his pioneering work in the field of replaceable foot.

REFERENCES

[1] Zhou, Y., Wu, H., Gu, A.Q.: Earthquake engineering: From earthquake resistance, energy dissipation, and isolation, to resilience, Engineering Mechanics, 36 (2019) 6, pp. 1-12.

[2] Lv, X.L., Chen, Y., Mao, Y.J.: New Concept of Structure al Seismic Design: Earthquake Resilient Structures, Journal of Tongji University (Natural Science), 39 (2011) 7, pp. 941-947.

[3] Lv, X.L., Quan, L.M., Jiang, H.J.: Research trend of earthquake resilient structures seen from 16WCEE, Earthquake engineering and engineering dynamics, 37 (2017) 3, pp. 1-9.

[4] Calado, L., Proenca, J. M., Espinha, M.: Hysteretic behavior of dissipative welded fuses for earthquake resistant composite steel and concrete frames, Steel and Composite Structures, 14 (2013) 6, pp. 547-569.

[5] Calado, L., Proenca, J. M., Espinha, M.: Hysteretic behavior of dissipative bolted fuses for earthquake resistant steel frames, Journal of Constructional Steel Research, 85 (2013), pp. 151-162.

[6] Chen, Y., Shao, T., He, X.: Study on steel H-beams with replaceable energy dissipation angle, Proceedings of the 8th International Symposium on Steel Structures. Korea: Korean Society of Steel Construction, pp. 369-370, 2015.

[7] Guo, W., Zeng, C.: A New Tuned Liquid Damper Applied in Building for Seismic Vibration Control. Structural Engineers, 34 (2018), pp. 59-66.

[8] Chen, M., Chen, B.W., Zou, Y.S.: Energy dissipation design of frame-supported shear wall structures. Building Structure, 46 (2016) 6, pp. 43-48.

[9] Hashemi, A., R. Masoudnia, P. Quenneville.: A numerical study of coupled timber walls with slip friction damping devices, Constr. Build. Mater., 121 (2016), pp. 373–385, https://doi.org/10.1016/j.conbuildmat.2016.05.160.

[10] Hashemi, A., P. Zarnani, R. Masoudnia, P. Quenneville.: Experimental testing of rocking cross-laminated timber walls with resilient slip friction joints. J. Struct. Eng., 144 (2018) 1, 04017180, https://doi.org/10.1061/(ASCE)ST.1943-541X.0001931.

[11] Yoshiaki, K., Hidemaru S., Koichiro I., Yasushi F., Solomon T.: Friction-based connectors for timber shear walls: static experimental tests, J. Archit. Eng., 25 (2019) 2, 04019006.

[12] Deng, K.L., Zheng D., Yang C., Xu T.F.: Experimental and Analytical Study of Fully Prefabricated Damage-Tolerant Beam to Column Connection for Earthquake-Resilient Frame, J. Struct. Eng., 145 (2019) 3, 04018264.

[13] Morgen, G.B., Kurama, C.Y.: Seismic Design of Friction-Damped Precast Concrete Frame Structures, Journal of Structural Engineering, 133 (2007) 11, pp. 1501-1511.

[14] Liu, Y.S., Han,J.P., Wang, X.Q.: Investigation on seismic performance of bridge with self-centreing friction dampers, Advanced Engineering Sciences, 50 (2018) 6, pp. 77–83.

[15] Liu, S.B., Li, A.Q.: Experimental study on a friction damper of aluminium foam/ pol0 yurethane interpenetrating phase composites, China Civil Engineering Journal, 50 (2018) 6, pp. 77–83.

[16] Zhang, Y.X., Huang, W.Z., Liu, A.Q.: A study on the behavior of self-centreing and free-repair braces with friction dampers. Journal of Vibration and Shock, 37 (2018) 4, pp. 126-146.

[17] Shi, Q.X., Wang, S.L., Su, S.Q., Wang, Q.W., Zhu, J.Q.: Pseudo-dynamic test of a reinforced concrete frame-shear wall model structure, China Civil Engineering Journal, 44 (2011) 7, pp. 1-9.

[18] Hung, C.C., Li, A.H., Chen, H.C.: High-strength steel reinforced squat UHPFRC shear walls: cyclic behavior and design implications, Engineering Structures, 141 (2017), pp. 59-74.

[19] Mohamed, N., Farghaly, A.S., Benmokrane, B.: Experimental investigation of concrete shear walls reinforced with glass fiber-reinforced bars under lateral cyclic loading, Journal of Composites for Construction, 18 (2014) 3, pp. 271-281.

[20] Mao, Y.J., Lv, X.L.: Quasi-static cyclic tests of RC shear wall with replaceable foot parts, Journal of Central South University (Science and Technology), 45 (2014) 6, pp. 2029-2040.

[21] Liu, Q.Z., Jiang, H.J.: Design Method of New Type of Reinforced Concrete Shear Wall with Replaceable Corner Components and Its Analysis, Journal of Tongji University (Natural Science), 44 (2016) 1, pp. 37-44.

[22] Lv, X.L., Mao, Y.J.: Design Method for RC Shear Walls with Replaceable Foot Parts, Structural Engineers, 28 (2012) 3, pp. 12-17.

[23] Qian, J.R., Xu, F.J.: Displacement-based deformation capacity design method of RC cantilever walls, J Tsinghua Univ (Sci& Tech), 47 (2007) 3, pp. 305-308.

[24] Yan, L.Z., Liang, X.W., Xu, J.: Research on Calculation Method of Deformation Capacity of Reinforced Concrete Shear Wall, Engineering Mechanics, 31 (2014) 11, pp. 92-98.

[25] Park, R., Paulay, T.: Reinforced Concrete Structures, New York: Wiley, 1975, pp. 535 - 553.

[26] Paulay, T., Priestley, M.J.N.: Seismic Design of Reinforced Concrete and Masonry Buildings, New York: John Wiley & Sons, Inc, 1992.

[27] Bohl, A., Adebar, P.: Plastic Hinge Lengths in High Rise Concrete Shear Walls, ACI Structural Journal, 108 (2011) 2, pp. 148-157.

[28] Wang, Y.J., Wang, M.F.: Study on Calculation Model of Plastic Hinge Length of Reinforced Concrete Shear Walls, Industrial Construction, 46 (2016) 5, pp. 80-85+165.

[29] Zhang, S., Lv, X.L., Zhang, H.M.: Experimental and analytical studies on the ultimate displacement of RC shear walls, China Civil Engineering Journal, 42 (2009) 4, pp. 10-16.

[30] Mehrdad, S., Armen, D.K.: Seismic Fragility of RC Structural Walls: Displacement Approach, Journal of Structural Engineering, ASCE, 127 (2001) 2, pp. 219-228.

[31] Wen, B.J., Liang, X.W.: Shear Capacity of Hinge Region of RC Shear Wall, Xi'an: Xi'an University of Architectural Science and Technology, 2008.

[32] Priestley, M.J.N.: Aspect of drift and ductility capacity of rectangular cantilever structural wall, Bulletin of New Zealand Society for Earthquake Engineering, 31 (1998) 2, pp. 73-85.

[33] Ministry of Housing and Urban-Rural Construction of the People's Republic of China.: Code for design of concrete structures (2015) (GB 50010-2010), Beijing: China Construction Industry Publishing House, 2016.

[34] Wei, Y.L., Pierre, Q., Nawawi, C.: A numerical study of the seismic behavior of timber shear walls with slip-friction connectors, Engineering Structures, 34 (2012), pp. 233-243.

[35] Lv, W., Qian, J.R., Fang, E.H.: Experimental and computational studies on ductility of reinforced concrete shear walls, J Tsinghua Univ (Sci& Tech), 39 (1999) 4, pp. 88-91.

[36] CSI Anaylsis Reference Manual For Sap2000, ETABS and SAFE, CSI, 2009.

[37] Wei Y. L., Pierre, Q., Nawawi, C.: A low damage and ductile rocking timber wall with passive energy dissipation devices, Earthquakes and structures, 9 (2015) 1, pp. 127-143.

[38] Xu, Z.L.: Elasticity, Beijing: Higher Education Press, 2016.

[39] MarcAndre, M., Krishan, K.C.: Mechanical Behavior of Materials (Second Edition). Cambridge: Cambridge University Press, 2009.

[40] Sun, X.F., Fang, X.S., Guan, L.: Mechanics of materials, Beijing: Higher Education Press, 2019.

[41] Wei Y.L., Pierre, Q., Nawawi, C.: Seismic behaviour of timber shear walls with load-limiting slip-friction connectors, The New Zealand Society for Earthquake Engineer (2009), Auckland,2009.

[42] Ministry of Housing and Urban-Rural Construction of the People's Republic of China. Specification for seismic test of buildings (JGJ/T101-2015), Beijing: China Construction Industry Publishing House,2015.

[43] Wang, S.L., Li, T., Yang, T., Zhang, B., Ju, J.: Experimental study on seismic behavior of RAC columns with silica fume and hybrid fiber, Journal of Building Strucruers, 34 (2013) 5, pp. 122-129.

[44] Clough, R., Penzien, J.: Dynamics of structures, Berkeley: Criticare Systems, Inc., 2004.